Subspace Classification of Human Gait Using Radar Micro-Doppler Signatures

Ann-Kathrin Seifert*, Lukas Schäfer, Moeness G. Amin†, Abdelhak M. Zoubir*

*Signal Processing Group
Technische Universität Darmstadt
64283 Darmstadt, Germany
{seifert, zoubir}@spg.tu-darmstadt.de

†Center for Advanced Communications
Villanova University
Villanova, PA 19085, USA
moeness.amin@villanova.edu

***Abstract*—Radar-based monitoring of human gait has become of increased interest with applications to security, sports biomechanics, and assisted living. Radar sensing offers contactless monitoring of human gait. It protects privacy and preserves a person's right to anonymity. Considering normal, pathological and assisted gait, we demonstrate the effectiveness of radar in discriminating different walking styles. By use of unsupervised feature extraction methods utilizing principal component analysis, we examine five gait classes using two different joint-variable signal representations, i.e., the spectrogram and the cadence-velocity diagram. Results obtained with experimental K-band radar data show that the choice of signal domain and adequate pre-processing are crucial for achieving high classification rates for all gait classes.**

I. Introduction

Gait analysis finds important applications in many areas such as sports biomechanics, medical diagnosis, and rehabilitation [1]. In the last two cases, the observation of gait serves as a basis for therapeutic interventions or ancillary examinations. In this respect, changes in gait patterns can serve as early indicators for neurological conditions, such as parkinsonism, orthopedic problems, and medical conditions.

Most of the research concerned with gait recognition is based on video analysis or wearable-sensor data, see e.g. [2]. On the other hand, radar as an electromagnetic sensing modality has proven to be suitable for analyzing the human gait, see e.g. [3]. It has the advantage of being insensitive to lighting conditions, environmental changes and clothing. Further, it enables remote monitoring of human gait in an unobtrusive and privacy-preserving manner. Due to the micro-Doppler (mD) effect [4], the back-scattered radar signals reflect the intricate characteristics of the observed motion.

Classification of human daily activities and discrimination between normal and abnormal gait strongly depend on the representation domain of the radar backscattering, as well as, the set of features extracted from such domain. Typically, the desired radar performance requires careful selection of the above two processing means, and is more so in the intra motion category classification problem at hand. We show that the choice of signal representations and adequate pre-processing is important prior to applying unsupervised feature extraction methods, such as, e.g., principal component analysis (PCA). The suitability of data representation domains for human motions, including fall, was recently investigated in [5], where the range information was taken into account. In this paper, we assess the suitability of cadence-velocity and time-frequency representations for gait classification based on PCA features. Further, we quantify the effect of pre-processing on the classification accuracy.

Prior work on radar-based human gait recognition is concerned with discriminating between walking with and without arm swinging [6]–[8], walking while holding an object [9], [10], considering different speeds of walking [11] or aim at discriminating individuals [12]. The effect of walking aids, such as a cane or a walker, on radar mD signatures has recently been studied in [13]–[19]. Using experimental K-band radar data of five different gait classes, including normal, pathological and assisted walks, we apply PCA, two-dimensional PCA (2D-PCA), and two-dimensional two-directional PCA (2D2D-PCA) for feature extraction and achieve a classification rate of 96%. The proposed approach outperforms existing works on radar-based human gait recognition, such as [13], [14], in terms of classification accuracy. We note that 2D2D-PCA was previously investigated on radar data of human gait by Li *et al.* in [9], where walking with and without carrying an object was analyzed. Based on local windows of the spectrogram they achieved a classification accuracy of 92.1% and 91.9% applying PCA and 2D2D-PCA, respectively. Further, Tivive *et al.* [8] applied 2D2D-PCA for dimensionality reduction of feature vectors obtained from the time-frequency domain for discriminating walking motions with and without arm swinging, where they achieved a classification rate of 91.3%.

We show that 2D-PCA outperforms standard PCA in terms of classification accuracy. The former is faster and avoids singularities when computing the inverse image covariance matrix, as the images are not vectorized prior to forming the data matrix. Further, we demonstrate that, in our case, 2D2D-PCA decreases the classification accuracy compared to using 2D-PCA. This effect is due to the fact that the considered joint-variable representations do not show discriminating characteristics along the Doppler frequency axis, and as a result, the obtained feature vectors using 2D2D-PCA do not add any meaningful information about the observed motions.

This work is supported by the Alexander von Humboldt Foundation, Bonn, Germany.

ISBN 978-90-827970-1-5 © EURASIP 2018

The remainder of the paper is structured as follows. Sec. II introduces different joint-variable representations of radar data of human gait. In Sec. III, the feature extraction methods based on PCA and its extensions are outlined. Sec. IV presents the experimental results based on K-band radar data, and final conclusion are given in Sec. V.

II. Radar Micro-Doppler Signatures of Human Gait

Since the radar return signal of human gait is highly non-stationary, we employ the spectrogram to show how the signal's power spectrum evolves over time. Given a discrete-time signal $s(n)$, the spectrogram is calculated as the squared magnitude of the short-time Fourier transform (STFT)

$$\mathrm{S}(n,k) = \left| \sum_{m=0}^{M-1} w(m) s(n+m) \exp\left(-j2\pi \frac{mk}{K}\right) \right|^2, \quad (1)$$

for $n = 0, \ldots, N-1$, where M is the length of the smoothing window $w(\cdot)$, k is the discrete frequency index with $k = 0, \ldots, K-1$, and $N, M, K \in \mathbb{N}$. Figs. 1(a) and (c) show spectrograms of two walking styles, where the amplitude is converted to dB-scale and the background noise is reduced via adaptive thresholding. In (a), a person is limping toward the radar system. We can identify the limping leg by the reduced maximal Doppler shift of every other mD stride signature. A cane-assisted walk is shown in (c), where the radar has a back-view on the person. Here, first, forth, and seventh mD signatures are solely due the cane's motion, since the cane is not aligned with any leg. Further details on radar mD signatures of human gait can be found in [13]–[15].

Another joint-variable representation for analyzing human gait is the cadence-velocity diagram (CVD) [11], [12], [15], [20], which is obtained by taking the Fourier transform of the spectrogram along each Doppler frequency bin as

$$\mathrm{C}(\epsilon,k) = \left| \sum_{n=0}^{N-1} \tilde{\mathrm{S}}(n,k) \exp\left(-j2\pi \frac{n\epsilon}{L}\right) \right|, \quad (2)$$

where $\epsilon = 0, \ldots, L-1, L \in \mathbb{N}$, is the cadence frequency, and $\tilde{\mathrm{S}}$ is the noise-reduced spectrogram as shown in Figs. 1(a) and (c). Contrary to the spectrogram, the CVD is a time-invariant representation, i.e., it does not depend on the initial phase of the gait cycle. It depicts the periodicity of body parts that move with the same velocity. Figs. 1(b) and (d) show the CVDs obtained from the spectrograms in (a) and (c), respectively. In (b), the CVD reveals a stride rate of approximately $0.9\,\mathrm{Hz}$. However, the stride rate is not well defined in some cane-assisted walks. For this reason, we define the mD repetition frequency f_{mD}, which represents the number of leg or cane signatures per second.

III. Feature Extraction based on Principal Component Analysis

For feature extraction, both two-dimensional signal representations, i.e., the spectrogram and the CVD, are considered as images denoted by $\mathbf{X}$. PCA can be used to learn intrinsic characteristics of data by finding a set of orthonormal basis that can be used to reconstruct the data by appropriate weighting. Using only a subset of the thus obtained basis the high-dimensional data can efficiently be represented in a lower dimensional subspace. In this case, we aim to describe the spectrogram or CVD images by a small number of features.

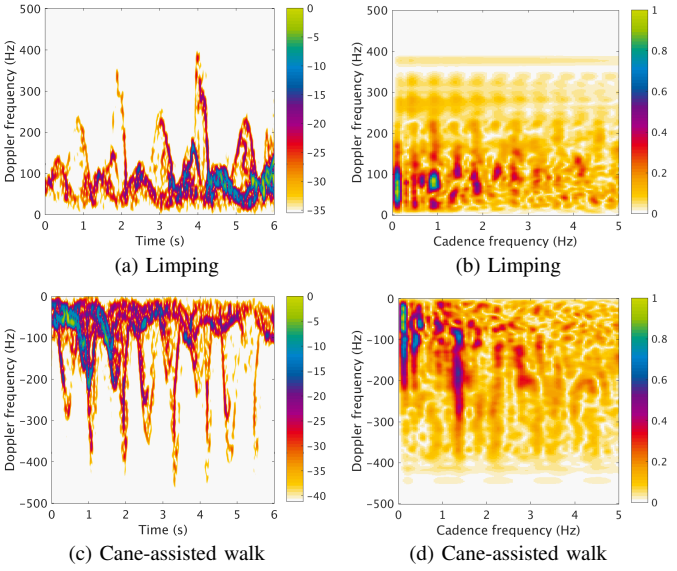

(a) Limping (b) Limping (c) Cane-assisted walk (d) Cane-assisted walk

Fig. 1. Examples of spectrograms for (a) limping with one leg, and (c) walking with a cane out of sync, along with the corresponding cadence-velocity diagrams in (b) and (d), respectively.

A. Principal Component Analysis

For PCA, the training images $\mathbf{X}_l \in \mathbb{R}^{I \times J}, l = 1, \ldots, P$ are vectorized row-wise, $\mathbf{x}_l = \mathrm{vec}\{\mathbf{X}_l^{\mathrm{T}}\} \in \mathbb{R}^{Q \times 1}$, and stacked column-wise to form a data matrix $\mathbf{Y}$, i.e., $\mathbf{Y} = [\mathbf{x}_1\ \mathbf{x}_2\ \cdots\ \mathbf{x}_P] \in \mathbb{R}^{Q \times P}$, where $Q = IJ$ is the total number of image pixels and P is the number of training images. The principal components are the eigenvectors of the covariance matrix of $\mathbf{Y}$ corresponding to the largest eigenvalues. For computing the principal components, the singular value decomposition (SVD) algorithm is utilized, which decomposes $\mathbf{Y}$ such that $\mathbf{Y} = \mathbf{U}\mathbf{D}\mathbf{V}^{\mathrm{T}}$, where the columns of $\mathbf{U}$ and $\mathbf{V}$ are the left and right eigenvectors, respectively. The diagonal matrix $\mathbf{D}$ contains the singular values on its main diagonal, where the eigenvalues are related to the singular values by $\mathbf{\Lambda} = 1/(P-1)\mathbf{D}^2$ [21]. The left eigenvector that corresponds to the largest eigenvalue is the first principal component and explains most of the variance in the data. The first α principal components span a α-dimensional subspace of the originally Q-dimensional data space. Each vectorized training and test image, $\mathbf{x}$, is projected into that subspace $\tilde{\mathbf{U}}$ by

$$\mathbf{p} = \tilde{\mathbf{U}}^{\mathrm{T}}\mathbf{x}, \quad (3)$$

where $\mathbf{p} \in \mathbb{R}^{\alpha \times 1}, \alpha \leq Q \in \mathbb{N}$ is the subspace representation of the original image. Here, $\tilde{\mathbf{U}} \in \mathbb{R}^{Q \times \alpha}$ contains the eigenvectors, or eigenimages, corresponding to the first α eigenvalues. The resulting projections $\mathbf{p} = [p_1\ p_2\ \cdots\ p_\alpha]^{\mathrm{T}}$, form the feature vector used for classification.

ISBN 978-90-827970-1-5 © EURASIP 2018

B. Two-dimensional Principal Component Analysis (2D-PCA)

Contrary to PCA, two-dimensional PCA operates on the image directly without prior vectorization [22]. From the image covariance matrix given by

$$\mathbf{H} = \frac{1}{P}\sum_{i=1}^{P}\left(\mathbf{X}_i - \bar{\mathbf{X}}\right)^{\mathrm{T}}\left(\mathbf{X}_i - \bar{\mathbf{X}}\right), \tag{4}$$

where $\bar{\mathbf{X}} = \frac{1}{P}\sum_{i=1}^{P}\mathbf{X}_i$ is the average training image, the optimal projection axes are found by maximizing the generalized total scatter criterion $J(\mathbf{\Phi}) = \mathbf{\Phi}^{\mathrm{T}}\mathbf{H}\mathbf{\Phi}$. The unitary vector that maximizes $J(\mathbf{\Phi})$, i.e., the eigenvector of $\mathbf{H}$ corresponding to the largest eigenvalue, gives the optimal projection axis. Let $\mathbf{\Phi}$ be the optimal projection matrix whose columns contain β optimal projection axes, i.e., $\phi_1, \ldots, \phi_\beta, \beta \leq J \in \mathbb{N}$, an image $\mathbf{X}$ is projected by

$$\mathbf{P} = \mathbf{X}\mathbf{\Phi}. \tag{5}$$

The obtained feature matrix $\mathbf{P} \in \mathbb{R}^{I\times\beta}$ is vectorized prior to classification.

C. Two-dimensional Two-directional Principal Component Analysis (2D2D-PCA)

The 2D-PCA operates along the row direction of the input images [23]. In order to take the information along the image columns into account, we calculate the image covariance matrix

$$\mathbf{V} = \frac{1}{P}\sum_{i=1}^{P}\left(\mathbf{X}_i - \bar{\mathbf{X}}\right)\left(\mathbf{X}_i - \bar{\mathbf{X}}\right)^{\mathrm{T}}, \tag{6}$$

where $\bar{\mathbf{X}} = \frac{1}{P}\sum_{i=1}^{P}\mathbf{X}_i$ is again the average training image. Maximizing the following generalized total scatter criterion $J(\mathbf{\Omega}) = \mathbf{\Omega}^{\mathrm{T}}\mathbf{V}\mathbf{\Omega}$, the optimal projection axes are given by the eigenvectors of $\mathbf{V}$. Using γ eigenvectors corresponding to the largest eigenvalues, we obtain γ optimal projection axes $\omega_1, \ldots, \omega_\gamma$, where $\gamma \leq I \in \mathbb{N}$. Let $\mathbf{\Omega}$ be the optimal projection matrix whose columns are given by $\omega_1, \ldots, \omega_\gamma$, the subspace representation of an image $\mathbf{X}$ is obtained by

$$\mathbf{P} = \mathbf{\Omega}^{\mathrm{T}}\mathbf{X}\mathbf{\Phi}. \tag{7}$$

The 2D2D-PCA feature matrix $\mathbf{P} \in \mathbb{R}^{\gamma\times\beta}$ is vectorized prior to classification.

IV. Experimental Results

A. Radar Data

The experimental radar data were recorded in an office environment at Technische Universität Darmstadt using a 24 GHz continuous-wave radar [24]. Four different test subjects were asked to walk toward and away from the radar system, covering a distance of approximately 4 m. The radar was positioned at 1.15 m above the ground. Each test subject performed five different walking styles: 1) normal walking (NW), 2) limping with one (L1) or 3) both legs (L2), 4) walking with cane in sync with one of the legs (CW), and 5) walking with a cane, where the cane is moved out of sync with any leg (CW/oos). In total, 400 measurements of 6 s duration are considered, where the number of experiments per gait class and direction are equal among the test subjects.

B. Methodology

The radar signals of length $N = 15360$ are processed to obtain the spectrogram as defined in Eq. (1), where a Hamming window of length $M = 255$ and $K = 2048$ discrete frequency points are used. After converting the spectrograms into logarithmic scale and suppressing the noise, the CVD is calculated according to Eq. (2) with $L = 2^{16}$ discrete frequency points. The spectrograms and the CVDs are considered as images and their pixel values are scaled to the range of $[0, 1]$, i.e., they are converted to gray-scale images. All images are resized to have the same size, with $I = 100$ and $J = 128$. The subspace is learned based on a subset of the available images. Here, 80% of the measurements are used for training, i.e., $P = 320$, and the remainder is used for testing. Projecting the training and test images into the subspace, we obtain features to train and test a classifier. The classification results are obtained using a simple nearest neighbor classifier with Euclidean distance. In order to assess the overall performance, 100 classification results are averaged, where training and test images are randomly chosen each time.

C. Comparison of Radar Data Representations

In order to demonstrate the importance of choosing appropriate data representations for feature extraction, we calculate the spectrograms and CVDs as described in Sec. II, and compare their classification performance. In order to compensate for the time dependence of the spectrogram, we extract four stride signatures per measurement and limit the Doppler axis to the maximal observed Doppler shift. We note that some gait spectrograms still show different initial stride types, e.g., the first step can be normal or abnormal.

Fig. 2(a) shows the classification accuracy over all gait classes as a function of the number of principal components using PCA-based features of spectrograms, time-aligned spectrograms and CVDs. Here, the shaded areas indicate $\pm\sigma$, where σ denotes the standard deviation of the classification accuracy. For the same number of principal components, the accuracy is significantly higher for the CVDs and aligned spectrograms compared to the raw spectrograms. In essence, using $\alpha = 18$ features CVDs and aligned spectrograms achieve an accuracy of approximately 90%, where the raw spectrograms reach only about 70% correct classification rate. The latter can be explained by the fact, that the raw spectrograms are not aligned in time and vary in the sequence and number of strides and (overlaying) cane signatures. Contrary to the spectrogam, the CVD depicts the motion patterns of the gait and is independent of the initial phase of the gait. Thus, we find that, for gait pattern recognition, the CVD is the preferred joint-variable representation.

D. Effect of Pre-Processing

CVDs represent the radar data in a joint frequency-frequency domain, i.e., Doppler and cadence frequency. From Fig. 1, we observe that along the Doppler frequency axis, the CVDs contain information up to the maximal observed Doppler shift. Hence, it is natural to consider the CVD

ISBN 978-90-827970-1-5 © EURASIP 2018

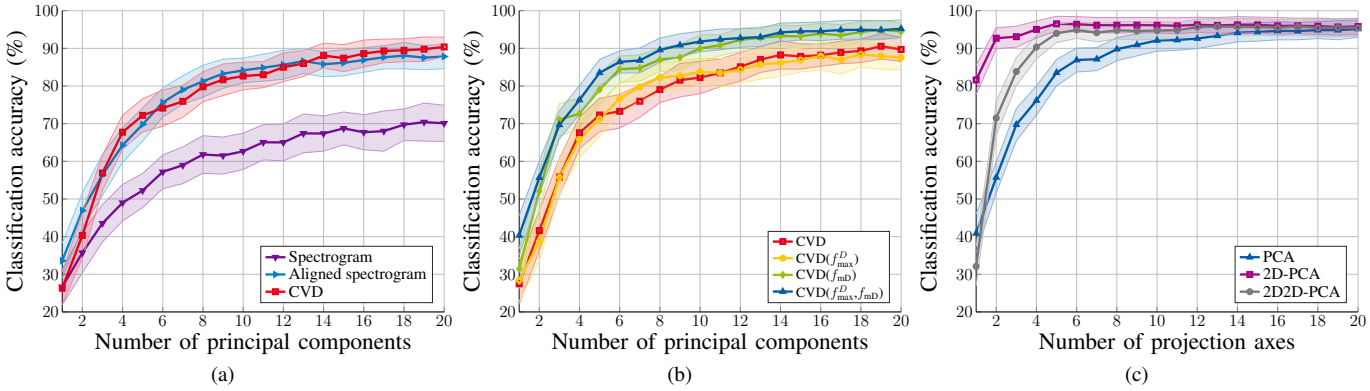

Fig. 2. Comparison of classification accuracy using (a) different input signals, (b) differently pre-processed CVDs, and (c) different feature extraction methods.

images only up to this limit. Further, walks vary in mD repetition frequency, where the amplitudes of the harmonic components decrease with increasing cadence frequency and the gait pattern is diminished beyond approximately 5 Hz. In order to assess the relevance of compensating for different maximal observed Doppler shifts $f^D_{\max}$ and mD repetition frequencies f_{mD}, we analyze the classification performance using the following pre-processed CVDs:

- CVD: considered up to ± 500 Hz Doppler frequency and 5 Hz cadence frequency,
- CVD($f^D_{\max}$): considered up to $f^D_{\max}$ and 5 Hz cadence frequency,
- CVD(f_{mD}): considered up to ± 500 Hz Doppler frequency and $5 \cdot f_{\mathrm{mD}}$ (Hz) cadence frequency
- CVD($f^D_{\max}$,f_{mD}): considered up to $f^D_{\max}$ and $5 \cdot f_{\mathrm{mD}}$ (Hz) cadence frequency,

where $f^D_{\max}$ and f_{mD} are extracted from the spectrogram as described in [13]. Fig. 3 shows examples of pre-processed CVDs, where (a) corresponds to the CVD in Fig. 1(d). We point out that pre-processing of CVDs along the cadence frequency axis was first proposed in [15].

The classification accuracy of using the aforementioned versions of the CVD and PCA-based feature extraction is shown in Fig. 2(b). It can be seen that compensating for different $f^D_{\max}$ does not significantly increase the classification performance compared to the raw CVD. However, aligning the CVDs along the cadence frequency axis, i.e., using CVD(f_{mD}) or CVD($f^D_{\max}$,f_{mD}), the classification accuracy is improved by 5% to 10% depending of the number of principal components.

E. PCA-based classification

Fig. 2(c) shows the classification results using PCA, 2D-PCA, and 2D2D-PCA for feature extraction of the pre-processed CVDs, i.e., CVD($f^D_{\max}$,f_{mD}). It can be seen that 2D-PCA outperforms PCA and 2D2D-PCA in terms of accuracy, when using only a small number of projection axes for feature extraction. Note that β is chosen equal to γ for 2D2D-PCA. The highest classification rates of 95.97% are achieved by using 2D-PCA and $\beta = 5$ projection axis. In Table I, the feature extraction methods are compared in terms of classification accuracy, dimension of the feature vector, and

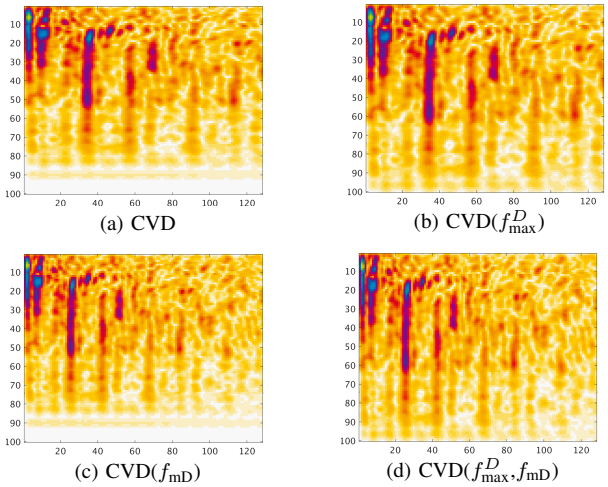

Fig. 3. Examples of pre-processed CVD images.

TABLE I
COMPARISON OF FEATURE EXTRACTION METHODS USING CVDS.

Method	Accuracy	Feature Dimension	Computation Time
PCA	83.21 %	5	0.57 s
2D-PCA	95.97 %	5×100	0.18 s
2D2D-PCA	93.53 %	5×5	0.16 s

computation time, where the latter is the average processing time over 100 classifications. Since the computation times of 2D-PCA and 2D2D-PCA are similar, we conclude that 2D-PCA is most efficient in capturing the inherent structure of the CVD.

In order to analyze why 2D2D-PCA does not outperform 2D-PCA, we compare the classification accuracy of using 2D-PCA on the pre-processed CVDs and the same images rotated by 90 degree. In essence, we compare the performance of using the image covariance matrix $\mathbf{H}$ of Eq. (4), or $\mathbf{V}$ of Eq. (6) for feature extraction. Fig. 4 shows that the classification accuracy is generally lower when using $\mathbf{V}$. This holds for both, the pre-processed CVDs and the aligned spectrograms. Hence, the rows of both joint-variable signal representations contain more information for discriminating different gait classes than their columns. In these cases, 2D2D-PCA does not outperform

ISBN 978-90-827970-1-5 © EURASIP 2018

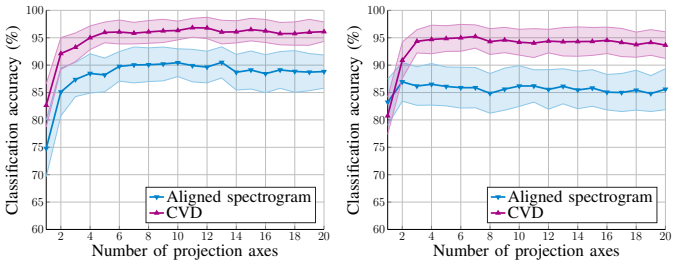

(a) 2D-PCA($\mathbf{H}$) (b) 2D-PCA($\mathbf{V}$)

Fig. 4. Comparison of classification performance for 2D-PCA using time-aligned spectrograms and pre-processed CVDs. In (b) the input images are rotated by 90 degree prior to feature extraction.

TABLE II
CONFUSION MATRIX (%) USING 2D-PCA AND ALIGNED SPECTROGRAMS.

True / Predicted	NW	L1	L2	CW	CW/oos
Normal walk (NW)	82	2	0	15	1
Limping with one leg (L1)	4	92	3	1	0
Limping with both legs (L2)	4	3	91	2	0
Cane - synchronized (CW)	13	1	0	85	1
Cane - out of sync (CW/oos)	2	2	1	3	92

TABLE III
CONFUSION MATRIX (%) USING 2D-PCA AND PRE-PROCESSED CVDS.

True / Predicted	NW	L1	L2	CW	CW/oos
Normal walk (NW)	97	0	0	3	0
Limping with one leg (L1)	1	98	0	1	0
Limping with both legs (L2)	2	0	93	5	0
Cane - synchronized (CW)	5	3	0	92	0
Cane - out of sync (CW/oos)	0	0	0	1	99

2D-PCA because of the special pattern in the images at hand.

The confusion matrices for 2D-PCA-based feature extraction using aligned spectrograms and pre-processed CVDs are given in Tables II and III, respectively. Here, the image covariance matrix $\mathbf{H}$ and $\beta = 5$ projection axes are used. The average accuracy over all gait classes is 88.56% and 95.97% for the spectrograms and the CVDs, respectively. Using spectrograms, most of the confusion appears between NW and CW, which is natural since the underlying gait pattern of a cane-assisted walk is a normal walk. However, the CVD is able to reduce this confusion significantly as it detects the additional periodicity in the gait due to the cane's motion.

V. CONCLUSION

We addressed the importance of choosing appropriate signal representations and perform adequate pre-processing prior to unsupervised feature extraction based on PCA and its extensions. We found that for radar-based human gait recognition, the CVD represents a more suitable joint-variable representation to discern different gait patterns than the spectrogram. Experimental results show that five different gait classes are correctly classified in 96% of the cases using pre-processed CVDs. Here, 2D-PCA is found most efficient for feature extraction compared to standard PCA and 2D2D-PCA.

REFERENCES

[1] W. Pirker and R. Katzenschlager, "Gait disorders in adults and the elderly: A clinical guide," *Wiener Klinische Wochenschrift*, vol. 129, no. 3, pp. 81–95, 2017.
[2] A. Muro-de-la Herran, B. Garcia-Zapirain, and A. Mendez-Zorrilla, "Gait analysis methods: an overview of wearable and non-wearable systems, highlighting clinical applications," *Sensors*, vol. 14, no. 2, pp. 3362–3394, 2014.
[3] M. G. Amin, Ed., *Radar for Indoor Monitoring: Detection, Classification, and Assessment*, CRC Press, 2017.
[4] V. C. Chen, *The Micro-Doppler Effect in Radar*, Artech House, 2011.
[5] B. Jokanovic and M. G. Amin, "Suitability of data representation domains in expressing human motion radar signals," *IEEE Geosci. Remote Sens. Lett.*, vol. 14, no. 12, pp. 2370–2374, 2017.
[6] B. G. Mobasseri and M. G. Amin, "A time-frequency classifier for human gait recognition," in *SPIE Defense, Security, and Sensing*, 2009.
[7] F. H. C. Tivive, A. Bouzerdoum, and M. G. Amin, "A human gait classification method based on radar Doppler spectrograms," *EURASIP J. Adv. Signal Process.*, vol. 2010, no. 1, pp. 389716, 2010.
[8] F. H. C. Tivive, S. L. Phung, and A. Bouzerdoum, "Classification of micro-Doppler signatures of human motions using log-Gabor filters," *IET Radar, Sonar & Navigation*, vol. 9, no. 9, pp. 1188–1195, 2015.
[9] J. Li, S. L. Phung, F. H. C. Tivive, *et al.*, "Automatic classification of human motions using doppler radar," in *Proc. IEEE Intern. Joint Conf. Neural Netw.*, 2012, pp. 1–6.
[10] F. Fioranelli, M. Ritchie, and H. Griffiths, "Aspect angle dependence and multistatic data fusion for micro-doppler classification of armed/unarmed personnel," *IET Radar, Sonar & Navigation*, vol. 9, no. 9, pp. 1231–1239, 2015.
[11] C. Clemente, L. Pallotta, A. D. Maio, *et al.*, "A novel algorithm for radar classification based on Doppler characteristics exploiting orthogonal pseudo-Zernike polynomials," *IEEE Trans. Aerosp. Electron. Syst.*, vol. 51, no. 1, pp. 417–430, 2015.
[12] R. Ricci and A. Balleri, "Recognition of humans based on radar micro-Doppler shape spectrum features," *IET Radar, Sonar & Navigation*, vol. 9, no. 9, pp. 1216–1223, 2015.
[13] A.-K. Seifert, A. M. Zoubir, and M. G. Amin, "Radar classification of human gait abnormality based on sum-of-harmonics analysis," in *Proc. IEEE Radar Conf.*, 2018, to be published, [Online-Edition: www.researchgate.net/publication/321587930].
[14] A.-K. Seifert, M. G. Amin, and A. M. Zoubir, "New analysis of radar micro-Doppler gait signatures for rehabilitation and assisted living," in *Proc. IEEE Int. Conf. Acoustics, Speech and Signal Process.*, 2017.
[15] A.-K. Seifert, A. M. Zoubir, and M. G. Amin, "Radar-based human gait recognition in cane-assisted walks," in *Proc. IEEE Radar Conf.*, 2017.
[16] M. S. Seyfioglu, A. M. Özbaygglu, and S. Z. Gurbuz, "Deep convolutional autoencoder for radar-based classification of similar aided and unaided human activities," *IEEE Trans. Aerosp. Electron. Syst.*, 2018, to be published.
[17] S. Z. Gurbuz, C. Clemente, A. Balleri, *et al.*, "Micro-Doppler-based in-home aided and unaided walking recognition with multiple radar and sonar systems," *IET Radar, Sonar & Navigation*, vol. 11, no. 1, pp. 107–115, 2017.
[18] M. G. Amin, F. Ahmad, Y. D. Zhang, *et al.*, "Micro-Doppler characteristics of elderly gait patterns with walking aids," *SPIE Defense + Security*, pp. 94611A–94611A, 2015.
[19] M. G. Amin, F. Ahmad, Y. D. Zhang, *et al.*, "Human gait recognition with cane assistive device using quadratic time-frequency distributions," *IET Radar, Sonar & Navigation*, vol. 9, no. 9, pp. 1224–1230, 2015.
[20] S. Björklund, H. Petersson, and G. Hendeby, "Features for micro-Doppler based activity classification," *IET Radar, Sonar & Navigation*, vol. 9, no. 9, pp. 1181–1187, 2015.
[21] I. Koch, *Analysis of Multivariate and High-Dimensional Data*, Cambridge University Press, 2013.
[22] J. Yang, D. Zhang, A. F. Frangi, *et al.*, "Two-dimensional PCA: a new approach to appearance-based face representation and recognition," *IEEE Trans. Pattern Anal. Mach. Intell.*, vol. 26, no. 1, pp. 131–137, 2004.
[23] D. Zhang and Z.-H. Zhou, "$(2D)^2$PCA: two-directional two-dimensional PCA for efficient face representation and recognition," *Neurocomputing*, vol. 69, no. 1, pp. 224 – 231, 2005.
[24] Ancortek Inc., "SDR-KIT 2400AD," http://ancortek.com/sdr-kit-2400ad, retrieved: 02/20/2018.

ISBN 978-90-827970-1-5 © EURASIP 2018